

Transport in the emergent Bose liquid: Bad metal, strange metal, and weak insulator, all in one system

Tao Zeng (曾涛),^{1,2} Anthony Hegg,¹
Long Zou (邹龙),^{1,2} Shengtao Jiang (蒋晟韬),^{1,2} Wei Ku (顧威)^{1,2,3*}

¹Tsung-Dao Lee Institute, Shanghai Jiao Tong University, Shanghai 200240, China

²School of Physics and Astronomy, Shanghai Jiao Tong University, Shanghai 200240, China

³Ministry of Education Key Laboratory of Artificial Structures and Quantum Control, Shanghai 200240, China

*To whom correspondence should be addressed; E-mail: weiku@mailaps.org.

Non-saturating high-temperature resistivity (“bad metal”), T -linear low-temperature resistivity (“strange metal”), and a crossover to activation-free growth of the resistivity in the low-temperature limit (“weak insulator”) are among the most exotic behaviors widely observed in many strongly correlated materials for decades that defy the standard Fermi liquid description of solids. Here we investigate these puzzling behaviors by computing temperature-dependent optical conductivity of an emergent Bose liquid and find that it reproduces all the unexplained features of the experiments, including a featureless continuum and a well-known mid-infrared peak. Amazingly and with physically intuitive mechanisms, the corresponding doping- and temperature-dependent resistivity displays the bad metal and strange metal simultaneously and sometimes weak insulating behaviors as well. The unification of all these non-Fermi liquid behaviors in a single model suggests that a new quantum state of matter, namely the emergent Bose liquid, will guide the development of the next generation of solid state physics.

Introduction Transport properties are among one of the most important features of materials widely used in many applications. Understandably, typical solid state physics textbooks start with the Drude model that provides a simple description of the transport properties of metals and lays the foundation of the Fermi liquid theory that constitutes most of the textbook knowledge. It

is therefore quite unsettling that, in strongly correlated materials, several atypical characteristics have been repeatedly observed for decades and yet consensus of reasonable understanding is still lacking. In essence, these exceptional features reflect the important fact that these materials are in some novel or exotic quantum states whose response defies the standard lore.

One well-known example is the so-called “bad metal” behavior (1,2), namely a non-saturating resistivity at high temperature beyond the Mott-Ioffe-Regel (MIR) limit (3), found in many strongly correlated materials such as some of the cuprates (4–9), vanadates (10), ruthenates (11, 12), and Rb_3C_{60} (13), to give a few examples in (Fig. 1)(a)(b). In standard theories, high-temperature resistivity originates from thermally enabled incoherent scattering of fermionic carriers (from disorder, phonon, or other carriers), and is directly related to the mean-free-path l^{MFP} (average distance between scatterings) of the carriers. The fact that l^{MFP} has a lower bound of the order of atomic distance implies an upper bound of resistivity, the MIR limit. Therefore, such a breach of MIR limit appears to imply a shorter l^{MFP} than atomic length scale, which is impossible given the very large Hartree scale energy level spacing inside an atom.

Another example of atypical transport is the so-called “strange metal” behavior (14), namely a temperature T -linear resistivity at low temperature, also discovered in many strongly correlated systems, including cuprates (14–16), twisted bi-layer graphene (17), iron pnictides (18), ruthenium oxides (19), organic metals (20), transition-metal dichalcogenides (21,22) and heavy-fermion compounds (23). [e.g. see T -linear resistivity of several materials in (Fig. 1)(a)]. This strange metal behavior is very difficult to understand from the standard picture of fermionic quasi-particles. Constrained by the Pauli principle of fermions, the key electron-electron scattering reduces dramatically as T approaches zero, with almost no phase space of scattering satisfying energy and momentum conservation. Therefore, in the absence of disorder the temperature dependent resistivity $\rho(T)$ should start at zero at $T = 0$ and grow with a power higher than linear, for example T^2 (24, 25) in the Fermi liquid theory (26). A T -linear resistivity thus suggests strongly that the fermionic quasi-particle picture is completely broken.

A third peculiar transport property at lower temperature is the so-called “weak insulating” behavior, where the metallic reduction of the resistivity crosses over to an insulator-like growth in the low-temperature limit. Most noticeably, this low-temperature resistivity growth $\rho(T)$ cannot be described by $e^{\Delta/T}$ as in typical insulators, indicating the lack of an activation energy scale Δ . [Some experimental data appears similar to $\ln(1/T)$ (29, 30).] Such a weak insulating behavior has been widely observed in many strongly correlated materials, including cuprates (29, 30), twisted bi-layer graphene (17), nickelates (31), iron pnictides (32), transition-metal dichalcogenides (21) and vanadium oxyselenides (33), to give a few examples. It is very puzzling how a coherent gapless fermionic quantum system displays smaller resistivity (weaker scattering) upon increasing temperature.

Perplexingly, the optical conductivity, which provides more complete dynamical information that should help shed light on these puzzles, suffers from yet more mysteries. For example, (Fig. 1)(c)(d) illustrate several features typically observed in the optical conductivity of such strongly correlated materials. First, there is an overwhelming continuum exhausting most of the spectral weight. Given the fact that optical conductivity corresponds to the long-wavelength

limit transport, one should instead expect the leading physics to be dominated by a Drude peak in the low-frequency limit of a one-band system such as shown here. Furthermore, since it takes $\sim eV$ frequency to access adjacent bands in this system, beyond the Drude peak there should be essentially no optical excitations up to this eV scale much less a dominant continuum. Second, some of these materials (28, 34) mysteriously show a clearly defined scale at mid-infrared frequencies ($\sim 100meV$) that is very insensitive to doping and temperature. This insensitivity rules out the relevance of observed scales, for example a superconducting gap, as an explanation for this phenomenon. Further, the scale of this feature ($\sim 100meV$) is incompatible with any well-understood scale in these materials such as a local repulsion $\sim 8eV$, charge transfer gap $\sim eV$, or antiferromagnetic interaction $\sim 150meV$. Finally, some features expected of the typical theories are instead completely absent. For example, if the superconducting gap is Δ_{SC} , then the optical conductivity should show a clear onset at energy $2\Delta_{SC}$, yet it has not been seen. It is hard to imagine how such a feature would not be observed in the optical conductivity if it is present in the underlying theory.

Armed with the knowledge that such unconventional phenomena are incompatible with theories reliant on fermionic quasiparticles, by far the dominant strategy to defeat conventional transport (35–39) utilizes some form of exotic scattering to disrupt the particle nature while retaining the fermionic description of the theory. Popular theories for the bad metal primarily incorporate thermal destruction of quasiparticles in strongly interacting systems such as via the Hubbard model (35, 36, 36, 37, 40, 40, 41), modified Hubbard model (38), and Mott quantum criticality (?). However, the local interaction scale is much too large ($\sim 8eV$) to generate the low-energy features (e.g. the $\sim 100meV$ onset of a continuum) in the optical conductivity. Breaking the quasiparticle nature is also the primary strategy in strange metal theories, which is typically achieved by introducing enough exotic scattering such as in marginal Fermi liquid (MFL) (42), anti-de Sitter space-conformal field theory (AdS-CFT) correspondence (39, 43), or quantum criticality (44–46). However, observations strongly indicate that T -linear resistivity (and more generally any power-law form for the resistivity) does not persist down to the lowest temperature scales, casting doubt on the applicability of such theories to a wide class of strongly correlated materials (47). Finally, the weak insulating behavior has been studied in the context of disorder scattering via bipolarons (48), Kondo-like physics (49), and pseudogap proximity (50). However, the wide range of temperature and doping where weak insulating behavior is found and its persistence in ever-cleaner samples (47) suggests that it is due to an intrinsic property of these systems over an equally wide parameter range.

Here we propose a different approach in which we retain the particle nature and instead replace the fermionic carriers with bosonic ones that emerge at some high energy scale. This choice is consistent with recent shot noise experiments on some of these materials (51, 52) identifying the carriers far away from the superconducting as having charge $2e$. Specifically, we study the temperature-dependent dynamical conductivity of an emergent Bose liquid (EBL) low-energy effective model (53–56). As an example, we apply this method to a square lattice of atoms. Surprisingly, our results closely resemble experimental observations reproducing all of the phenomena described above semi-quantitatively: bad metal, strange metal, weak insulator,

and all the essential features of the optical conductivity. More interestingly, as generic features of the EBL picture, each phenomenon has a clear and simple physical explanation. Our results lend compelling support to the scenario in which many of these strongly correlated materials are dominated by a new quantum state of matter: the emergent Bose liquid.

Main Text The conditions resulting in an EBL (53–56) are quite general and begin with a strong intra-atomic repulsion with corresponding short-range correlations at high energy. If we then assume that a binding mechanism becomes relevant at somewhat lower energy, then at even lower energy the physics will be dominated by bosons formed from nearest neighbor carriers. These bosons have centers at the bonds of the underlying fermion lattice, and they also have extended hardcores forbidding occupation of their surrounding bounds due to the high energy constraint. As illustrated below, an essential feature of such an EBL is the multi-orbital nature associated with the multiple bond orientations in 2D and 3D systems. Such multi-orbital nature of the EBL has recently been shown (56) to enable, when combined with geometrical frustration, a novel homogeneous Bose metal phase resembling (57) the pseudogap phase found in several strongly correlated materials.

As an example we consider a simple square lattice of fermions (as found in e.g. the cuprates, nickelates, ruthenates, etc). The corresponding bond-centered lattice of bosons form a checker-board lattice illustrated in (Fig. 2)(a)

$$H = \sum_{\langle l, l' \rangle} \tau_{ll'} b_l^\dagger b_{l'} \quad (1)$$

where b_l denotes the annihilation of a boson located at bond l with corresponding extended hardcore constraint [denoted by the yellow region in panel (a)], and $\tau_{ll'} = \tau'$ or τ'' is the fully dressed kinetic process involving nearest and second nearest neighboring bonds extracted from ARPES dispersion data previously (53).

We evaluate the optical conductivity via the Kubo formula

$$\sigma_{\alpha\beta}(\omega) = \frac{i}{\omega} [\Pi_{\alpha\beta}(\omega) + \frac{n_0 e^2}{m} \delta_{\alpha\beta}], \quad (2)$$

where $\Pi_{\alpha\beta}(\mathbf{q}, \tau) = -\frac{1}{\nu} \langle T_\tau j_\alpha^\dagger(\mathbf{q}, \tau) j_\beta(\mathbf{q}, \tau) \rangle$ is the current-current correlation function for α and β current components. Here, we focus on temperatures higher than the superconducting transition in the low-density regime and treat the influence of the hardcore constraint as negligible for long-wavelength ($q \rightarrow 0$) physics.

To help visualize the main features of the spectrum for this EBL and to reveal the physics unrelated to the typical temperature dependent scattering, we introduce a temperature- (and doping-) independent broadening η to σ for contributions from the low-energy band $\eta_1 \sim 30\text{meV}$ and the shorter-lived contributions from the high-energy band $\eta_2 \sim 10\eta_1$. As a matter of fact, as outlined in the supplementary, many strongly correlated materials exhibiting the exotic phenomena discussed here display a nearly temperature-independent broadening. This

could be understood if the dominant scattering channel originates from a high energy constraint such as via disorder, charge correlations in the TMDs, or magnetic correlations in the cuprates for example. As shown below, such a simple fixed scattering rate alone manages to produce these exotic phenomena in the EBL, so a temperature dependent scattering rate is not mandatory to understand these observations.

Figure 2(c) illustrates our result, which shows phenomenal agreement with experiments above the superconducting transition e.g. in panel (d). In particular, we find all of the puzzling phenomena discussed above including a featureless continuum spanning a large frequency range, a mid-infrared feature around 100meV, no sign of any superconductivity-related $2\Delta_{SC}$ feature.

The EBL effortlessly provides an explanation for all of these exotic puzzles. A broad featureless continuum over the entire frequency range originates from the gapless inter-band transitions [green arrows in (Fig. 2)(b)]. It is gapless because the two bands touch due to symmetry and all bosons participate due to a lack of a Pauli principle. Conspicuously, a mid-infrared feature $\sim 100\text{meV}$ rises out of this continuum due to the transitions between the two van-Hove singularities (red arrow). These van-Hove singularities are very weakly doping dependent, in excellent agreement with observation (28). In essence, the bond-centered lattice reveals a scale hidden in the kinetic energy of the underlying fermionic lattice. Finally, the lack of a superconducting gap signature around $2\Delta_{SC}$ is self-evident in a system of bosons. Since the bosonic band structure generates superfluidity without opening a gap, an onset at the $2\Delta_{SC}$ gap scale should not occur. Crucially, all of these features are made possible by the two-orbital nature of this example. As described above, multi-orbital bosonic models are a necessary outcome of the EBL scenario, so these features are inescapable consequences of any EBL.

Having unveiled all of the puzzles in the optical conductivity, we are now in a position to examine all of the exotic behaviors of the resistivity by simply taking the DC-limit ($\omega \rightarrow 0$) above the BEC transition. Interestingly, our result in (Fig. 3)(a) displays excellent agreement with experiments in (b) over a wide range of temperature and doping. In particular, we find the linear resistivity (strange metal) over a broad temperature range with a slope that decreases as doping increases. Deviation from this linear behavior (weak insulator) occurs at lower temperatures just above the superconducting transition, and saturation does not occur (bad metal) at any temperature within the study.

This exotic transport is as simple to understand as the optical conductivity used to obtain it. The dominant temperature and doping dependence of the optical conductivity $\sigma(T, x) \propto \int d^3k D_k(T, x)$ comes from

$$D_k(T, x) \propto \left. \frac{dn_B(\omega)}{d\omega} \right|_{\omega=\epsilon_k}. \quad (3)$$

Here n_B is the Bose-Einstein distribution and ϵ_k is a bosonic excitation energy for momentum k . Representing the resistivity via a typical component ρ_k we obtain

$$\rho_k(T, x) \propto D_k^{-1} \approx k_B T \sinh^2 \left(\frac{\epsilon_k - f(x)}{2T} + \frac{c}{x} \right), \quad (4)$$

where we have used the fact that the leading order temperature T - and density x -dependence of the chemical potential is $\mu \approx -c(T - T_c)/x$ for $T > T_c$, c is a constant, and $f(x)$ is a dimension-dependent function of density.

For example, the strange metal behavior necessarily results at high enough temperature with Eq.(4) becoming more T -linear as temperature is increased. In fact, a very careful analysis of the experimental data confirms that, contrary to popular belief, T -linear resistivity is not a low-temperature limit phenomenon. To illustrate this clearly we show the observed transverse and longitudinal resistivity in (Fig. 3)(d) and benchmark it in (c) against our formula Eq.(4). Particularly, transverse conductivity becomes asymptotically linear at higher temperature in both experiment and theory. This distinguishes such observations and our theory from many of the existing purely quantum mechanisms dominated by power-law scaling at low temperature (MFL, quantum criticality, AdS-CFT, etc.).

Furthermore, Eq.(4) suggests a simple doping dependent slope of the T -linear resistivity

$$\gamma(x) \equiv \frac{\partial \rho}{\partial T} \propto \sinh^2 \left(\frac{c}{x} \right). \quad (5)$$

Figure 3(e) compares the observed slopes (47) (red dots) with our numerical result (black squares), both fit remarkably well by Eq.(5) (blue curve) up to a *doping-independent* constant γ_0 reminiscent of phonon or magnon contributions.

Similarly, the weak insulating behavior necessarily results at low enough temperature with Eq.(4) becoming more divergent as temperature is further decreased. Figure 3(f) shows that a typical observation (59) of weak insulating behavior is fit precisely by Eq.(4) over multiple decades of temperature range spanning multiple qualitative characteristics. This fitting clearly goes far beyond the accuracy of the infamous $\ln(1/T)$ fitting, which covers less than half a decade in the inset of panel (f). This is a natural result in the EBL at low-temperature where the bosons are confined to low-energy and therefore systematically lose their velocity. Consequently, the seemingly 'insulating' behavior in a fermionic interpretation is in fact a generic low-temperature *metallic* behavior of an EBL.

Finally, the bad metal behavior is inevitable in Eq.(4) with unbounded resistivity as temperature is increased. It turns out that the continually growing resistivity in Eq.(4) is a result of the reduction of carrier density at low frequency and is correspondingly accompanied by a weight transfer to a higher frequency regime. Indeed, (Fig. 4)(a) shows (in light blue) that the fraction $f(T)$ of the integrated low-frequency spectral weight, up to some cutoff frequency $\omega_c = 500 \text{ cm}^{-1}$: $f = \int_0^{\omega_c} \sigma d\omega / \int_0^{\infty} \sigma d\omega$, continuously decreases as temperature grows. Note that the frequency range of weight transfer is rather large (larger than 100meV but smaller than 500meV), since a higher frequency cutoff ($\omega_c = 1000 \text{ cm}^{-1}$) shows a similar trend. Amazingly, the exact same behavior has been observed in recent experiments (28) as shown in (Fig. 4)(b). This weight transfer mechanism is completely distinct from the scattering-dominated considerations of fermionic systems from which the MIR limit is derived (3). Because of the constrained phase space allowed by the Pauli principle, it is virtually impossible for a fermionic system to develop this dramatic range of weight transfer.

We stress that all these transport features are yet again made possible by the multi-orbital nature of the EBL. In contrast, when constrained by an optical sum rule, a single orbital system does not have the flexibility of weight transfer to high energy. Consequently, at temperatures small compared to the bandwidth, only weakly temperature dependent resistivity would result under a fixed scattering rate. Incorporating this multi-orbital nature into the physics distinguishes the EBL from the standard bosonic pictures (60–62). The simple particle nature of these ‘exotic’ phenomena within the EBL paradigm offers it strong support as a universal low-energy model for a large class of strongly-correlated materials.

The excellent comparison between this square lattice example of the EBL and the cuprates supports its use as an appropriate low-energy model for the charge dynamics. Indeed, the known high-energy physics of the cuprates naturally fits into the basic assumptions of the EBL. The intra-atomic repulsion $\sim 8\text{eV}$ of the cuprates and the short-range antiferromagnetic correlation $\sim 150\text{meV}$ are both well-beyond the relevant energy scales in this study and therefore provide adequate high energy constraints. Furthermore, numerous strong binding mechanisms have been proposed for the cuprates with energy scales higher than room temperature, including via two-dimensional short-range antiferromagnetic correlation (63–65) and bi-polaronic correlation (66). Such excellent agreement suggests that the EBL dominates the charge dynamics of the most actively studied part of the phase diagram for the cuprates.

In summary, we demonstrate the bad, the strange, and the weak insulating behaviors above the superfluid phase in one emergent Bose liquid as a universal paradigm for transport properties in solids complementary to the textbook Fermi liquid theory. Instead of relying on exotic scattering to destroy the fermionic particle nature, the exploitation of bosonic characteristics combined with a multi-orbital picture allows uncomplicated particle-based mechanisms far from criticality to explain many long-standing puzzles in a wide range of strongly correlated materials. By providing a very intuitive physical understanding of not only the DC transport behaviors but even the exotic dynamics in the optical conductivity, we help the community circumvent the need to resort to arcane theoretical description such as that found in ‘quantum supreme matter’ (67). Applications of the EBL will greatly benefit basic science research by guiding a new generation of solid state physics and benefit technological development by facilitating the engineering and optimization of functional quantum materials.

References

1. V. J. Emery, S. A. Kivelson, *Phys. Rev. Lett.* **74**, 3253 (1995).
2. O. Gunnarsson, M. Calandra, J. E. Han, *Rev. Mod. Phys.* **75**, 1085 (2003).
3. N. Hussey, K. Takenaka, H. Takagi, *Philosophical Magazine* **84**, 2847 (2004).
4. N. L. Wang, C. Geibel, F. Steglich, *Physica C: Superconductivity* **262**, 231 (1996).
5. N. L. Wang, B. Buschinger, C. Geibel, F. Steglich, *Phys. Rev. B* **54**, 7445 (1996).

6. H. Takagi, *et al.*, *Phys. Rev. Lett.* **69**, 2975 (1992).
7. J. Orenstein, *et al.*, *Phys. Rev. B* **42**, 6342 (1990).
8. S. Martin, A. T. Fiory, R. M. Fleming, L. F. Schneemeyer, J. V. Waszczak, *Phys. Rev. B* **41**, 846 (1990).
9. K. Takenaka, J. Nohara, R. Shiozaki, S. Sugai, *Phys. Rev. B* **68**, 134501 (2003).
10. M. M. Qazilbash, *et al.*, *Phys. Rev. B* **74**, 205118 (2006).
11. P. Khalifah, *et al.*, *Nature* **411**, 669 (2001).
12. A. W. Tyler, A. P. Mackenzie, S. NishiZaki, Y. Maeno, *Phys. Rev. B* **58**, R10107 (1998).
13. A. F. Hebard, T. T. M. Palstra, R. C. Haddon, R. M. Fleming, *Phys. Rev. B* **48**, 9945 (1993).
14. A. Legros, *et al.*, *Nature Physics* **15**, 142 (2019).
15. R. Daou, *et al.*, *Nature Physics* **5**, 31 (2009).
16. R. A. Cooper, *et al.*, *Science* **323**, 603 (2009).
17. Y. Cao, *et al.*, *Phys. Rev. Lett.* **124**, 076801 (2020).
18. S. Kasahara, *et al.*, *Phys. Rev. B* **81**, 184519 (2010).
19. S. A. Grigera, *et al.*, *Science* **294**, 329 (2001).
20. N. Doiron-Leyraud, *et al.*, *Phys. Rev. B* **80**, 214531 (2009).
21. S. Sahoo, U. Dutta, L. Harnagea, A. K. Sood, S. Karmakar, *Phys. Rev. B* **101**, 014514 (2020).
22. B. Sipos, *et al.*, *Nature Materials* **7**, 960 (2008).
23. P. Gegenwart, Q. Si, F. Steglich, *Nature Physics* **4**, 186 (2008).
24. H. K. Pal, V. I. Yudson, D. L. Maslov, *Lithuanian Journal of Physics* **52**, 142 (2012).
25. N. P., D. Pines, *The Theory of Quantum Liquids (Advanced Book Classics)* (Perseus Books, LLC, 1999).
26. *Collected Papers of L.D. Landau*, D. T. HAAR, ed. (Pergamon, 1965), pp. 171–183.
27. Z. Fisk, G. W. Webb, *Phys. Rev. Lett.* **36**, 1084 (1976).
28. J. Hwang, T. Timusk, G. D. Gu, *Journal of Physics: Condensed Matter* **19**, 125208 (2007).

29. Y. Ando, G. S. Boebinger, A. Passner, T. Kimura, K. Kishio, *Phys. Rev. Lett.* **75**, 4662 (1995).
30. S. Ono, *et al.*, *Phys. Rev. Lett.* **85**, 638 (2000).
31. Q. Li, *et al.*, *Communications Materials* **1**, 16 (2020).
32. S. C. Riggs, *et al.*, *Phys. Rev. B* **79**, 212510 (2009).
33. H. Lin, *et al.*, *Phys. Rev. B* **98**, 075132 (2018).
34. T. Startseva, *et al.*, *Phys. Rev. B* **59**, 7184 (1999).
35. X. Deng, *et al.*, *Phys. Rev. Lett.* **110**, 086401 (2013).
36. N. Pakhira, R. H. McKenzie, *Phys. Rev. B* **91**, 075124 (2015).
37. E. Perepelitsky, *et al.*, *Phys. Rev. B* **94**, 235115 (2016).
38. C. H. Mousatov, I. Esterlis, S. A. Hartnoll, *Phys. Rev. Lett.* **122**, 186601 (2019).
39. T. Faulkner, N. Iqbal, H. Liu, J. McGreevy, D. Vegh, *Science* **329**, 1043 (2010).
40. J. Vučićević, D. Tanasković, M. J. Rozenberg, V. Dobrosavljević, *Phys. Rev. Lett.* **114**, 246402 (2015).
41. A. Georges, G. Kotliar, W. Krauth, M. J. Rozenberg, *Rev. Mod. Phys.* **68**, 13 (1996).
42. C. M. Varma, P. B. Littlewood, S. Schmitt-Rink, E. Abrahams, A. E. Ruckenstein, *Phys. Rev. Lett.* **63**, 1996 (1989).
43. S. Sachdev, *Journal of Statistical Mechanics: Theory and Experiment* **2010**, P11022 (2010).
44. S. Sachdev, *physica status solidi (b)* **247**, 537 (2010).
45. S. Sachdev, B. Keimer, *Physics Today* **64**, 29 (2011).
46. C. H. Mousatov, E. Berg, S. A. Hartnoll, *Proceedings of the National Academy of Sciences* **117**, 2852 (2020).
47. J. Wu, A. T. Bollinger, X. He, I. Bozovic, *Nature* **547**, 432 EP (2017).
48. A. S. Alexandrov, *Physics Letters A* **236**, 132 (1997).
49. F. B. C. P. F. Rullier-Albenque, H. Alloul, *Europhysics letters* **81**, 37008 (2008).
50. F. Laliberte, *et al.*, *arXiv e-prints* (2016).

51. P. Zhou, *et al.*, *Nature* **572**, 493 (2019).
52. K. M. Bastiaans, *et al.*, *arXiv e-prints* (2021).
53. Y. Yildirim, W. Ku, *Phys. Rev. X* **1**, 011011 (2011).
54. Y. Yildirim, W. Ku, *Phys. Rev. B* **92**, 180501 (2015).
55. Z.-J. Lang, F. Yang, W. Ku, *arXiv e-prints* (2019).
56. A. Hegg, J. Hou, W. Ku, *Proceedings of the National Academy of Sciences* **118**, e2100545118 (2021).
57. X. Yue, A. Hegg, X. Li, W. Ku, *arXiv e-prints* (2021).
58. Y. Ando, S. Komiya, K. Segawa, S. Ono, Y. Kurita, *Phys. Rev. Lett.* **93**, 267001 (2004).
59. Y. Ando, A. N. Lavrov, S. Komiya, K. Segawa, X. F. Sun, *Phys. Rev. Lett.* **87**, 017001 (2001).
60. M. P. A. Fisher, P. B. Weichman, G. Grinstein, D. S. Fisher, *Phys. Rev. B* **40**, 546 (1989).
61. A. S. Alexandrov, *Phys. Rev. B* **48**, 10571 (1993).
62. R. G. Leigh, P. Phillips, T.-P. Choy, *Phys. Rev. Lett.* **99**, 046404 (2007).
63. V. J. Emery, *Phys. Rev. B* **14**, 2989 (1976).
64. J. E. Hirsch, *Phys. Rev. Lett.* **54**, 1317 (1985).
65. M. P. M. Dean, *et al.*, *Nature Materials* **12**, 1019 EP (2013).
66. A. S. Alexandrov, N. F. Mott, *Reports on Progress in Physics* **57**, 1197 (1994).
67. J. Zannen (Physics Colloquium at University of Illinois at Urbana Champaign, 2020).

Acknowledgements We thank Jie Wu, Fan Yang, Zhi Wang, Zi-Jian Lang and Ruoshi Jiang for useful discussions. This work is supported by National Natural Science Foundation of China Grants 11674220 and 12042507.

Nearly temperature-independent scattering rate in observations of prototypical materials: A caution against fitting procedures accounting only for partial contribution

We focus on a material below with an optical conductivity spectrum characteristic of those in this study and argue that it is roughly consistent with temperature-independent scattering at high temperature, which justifies this decision in the manuscript. Surprisingly, some of the literature for these examples conclude that there is a strongly temperature-dependent scattering rate based on a very sophisticated fitting to e.g. a multiple component Drude model. Any such fitting based on partial contribution procedure should be treated with caution.

A typical example of the optical conductivity in these materials is illustrated in (Fig. S1). Our study aims to explain the transport properties above the superconducting transition temperature T_c , so we are primarily interested in comparing the optical response e.g. between 130K and 300K. Aside from the ever-present continuum and the oft-encountered mid-infrared feature at lower temperatures, we see a single peak centered around the DC-limit that is very broad. Most importantly, the width of this feature changes very little even when the temperature more than doubles.

To illustrate this insensitivity to temperature more clearly, we have inserted ‘width’ estimates for this feature, which clearly indicate that the relative change in width is much smaller than the relative change in temperature. Although the temperature-independent broadening used in the main text is chosen primarily to study the properties of the EBL independent of scattering details, optical conductivity observations such as here and in the additional materials illustrated below seem to be well-represented by such a simple broadening.

At first glance, the decision to use a temperature-independent broadening seems to contradict statements made in the publication originally containing the experimental data. For example, in the article corresponding to (Fig. S1) (*I*), it is claimed that ‘There is a Drude term which narrows progressively with decreasing temperature with a scattering rate following the transport properties...’. However, on closer inspection of the article, it is clear that such statements are made in reference to results after fitting the optical conductivity to a phenomenological Drude model.

Since the transport properties of these materials bear little-to-no resemblance to those of a standard metal, a simple Drude formula cannot capture the essence of the optical response. As a result, any use of such a formula to fit such qualitatively different data inevitably introduces an ad-hoc component that dominates the behavior of the function. In the example presented here the authors fit the data to a three-component function consisting of two qualitatively different Drude terms and a mid-infrared harmonic oscillator (*I*). Using a non-trivial ad-hoc parameterization to fit one set of data to a model designed to explain qualitatively dissimilar behavior can be useful to compare different observations but should be treated with great caution. In

particular, any physical conclusions drawn from such a procedure should be treated with great skepticism.

Avoiding the danger identified above, we take the more modest approach described at the beginning of this section and estimate the broadening based on properties of the clearly visible features of the data in absence of any particular model. Here and in the examples below we find it very reasonable to assume relatively temperature independent broadening in the regime valid to our study. Below we show examples of strongly correlated materials that exhibit qualitatively similar optical response with a low-frequency feature that is relatively insensitive to temperature over a large high-temperature range.

The optical conductivity for cuprate LSCO (2) is illustrated in (Fig. S2). It shows a FWHM that changes very little from e.g. 200K up to room temperature.

The optical conductivity for iron-based superconductor LaFePO (3) is illustrated in (Fig. S3). It has a FWHM that changes very little from e.g. 250K up to room temperature.

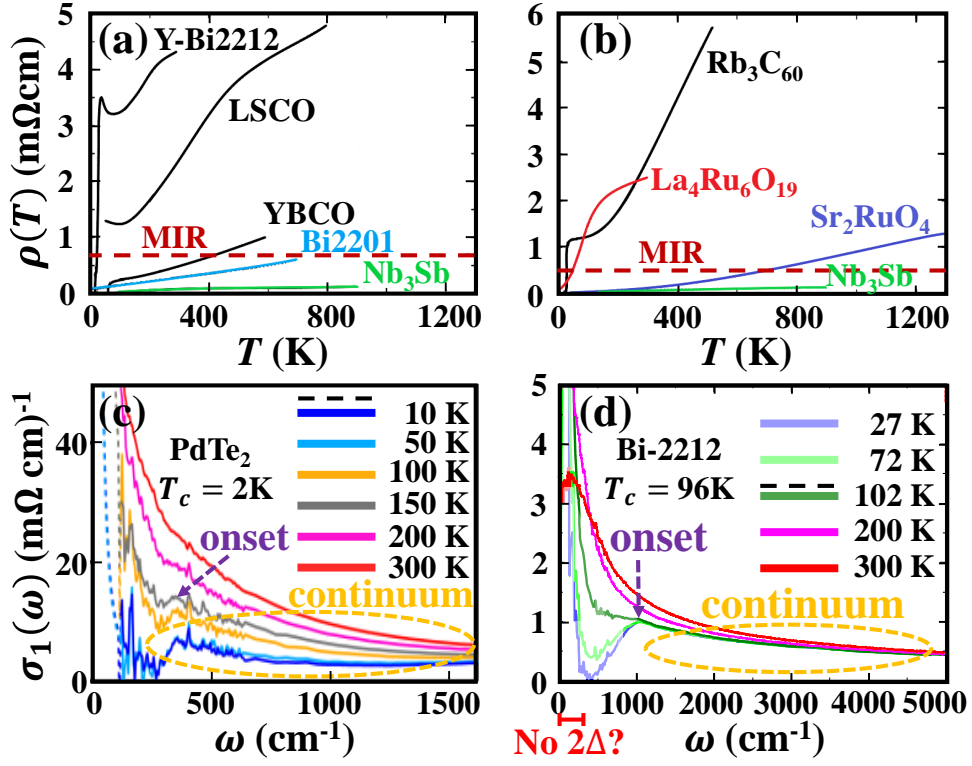


Figure 1: Temperature-dependent resistivity for several (a) cuprate (4–8) and (b) non-cuprate (11–13) strongly correlated materials with characteristic T -linear resistivity ranges and complete ignorance of the MIR saturation bound (red dotted lines). For comparison, Nb₃Sb (27) satisfies the MIR saturation condition (2). (c) Optical conductivity of PdTe₂ with ever-present continuum (orange dotted circle). A temperature-independent mid-infrared peak becomes visible at low temperature (purple dotted arrow). (d) Optical conductivity of Bi-2212 (28) with strongly similar features to (c) apart from a different overall scale.

References

1. V. Vescoli, L. Degiorgi, H. Berger, L. Forro, *Synthetic Metals* **103**, 2655 (1999).
2. S. Tajima, *et al.*, *Phys. Rev. B* **71**, 094508 (2005).
3. M. M. Qazilbash, *et al.*, *Nature Physics* **5**, 647 (2009).

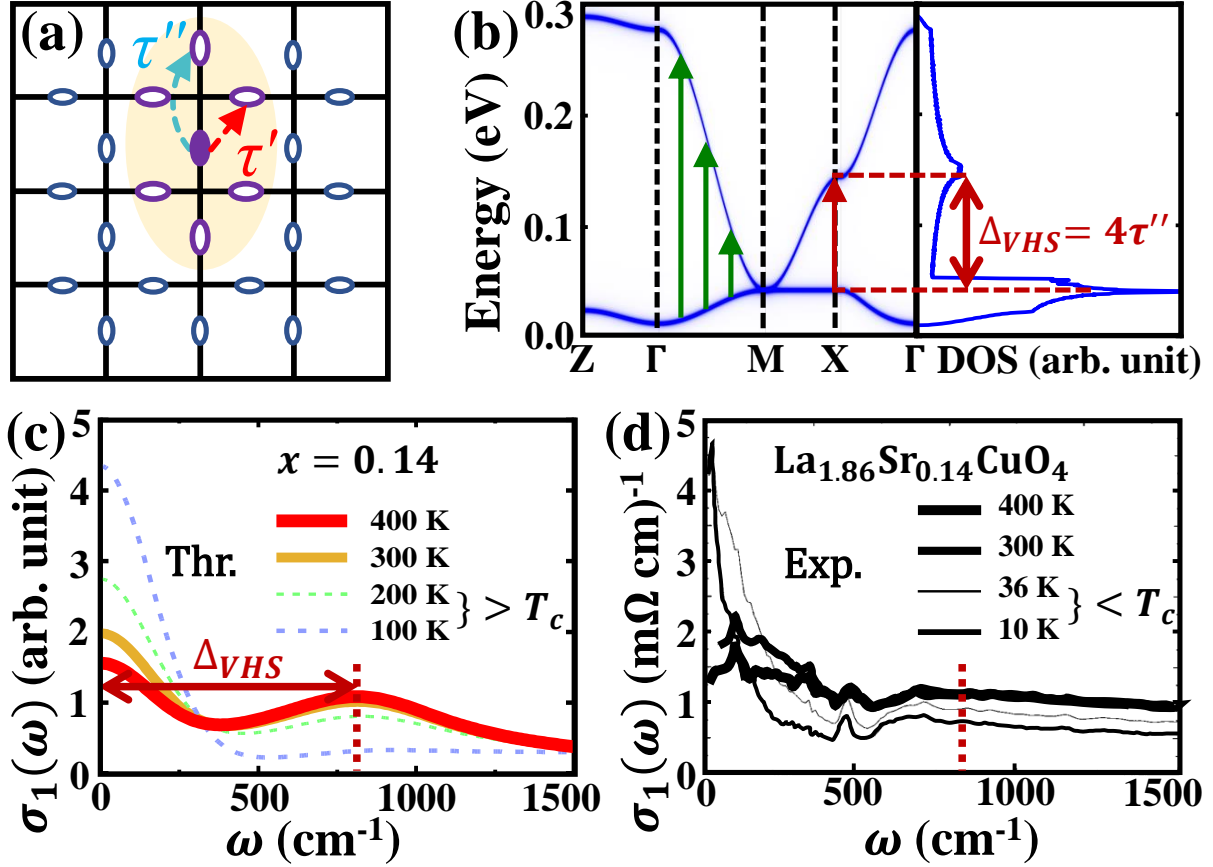


Figure 2: (a) Illustration of the emerged checkerboard lattice upon binding neighbor holes. In this emergent Bose liquid (EBL), a boson can hop to nearest or next-nearest neighbor sites by pivoting motion. The two different bond-centered orbitals are distinguished by horizontal and vertical boson orientations respectively. (b) The corresponding band structure and density of states of the EBL. At the Brillouin zone edge there are two van-Hove singularities. Green arrows illustrate possible inter-band excitations. (c) Optical conductivity computed in the emergent Bose liquid model and (d) corresponding experimental observation in LSCO (34) with amazing semi-quantitative agreement above the superconducting transition. A continuum is always observed in all cases, and the temperature dependence agrees at both high and low frequency. Notice the mid-infrared peak (red dotted lines) corresponds to the energy difference of the two van-Hove singularities (red arrows).

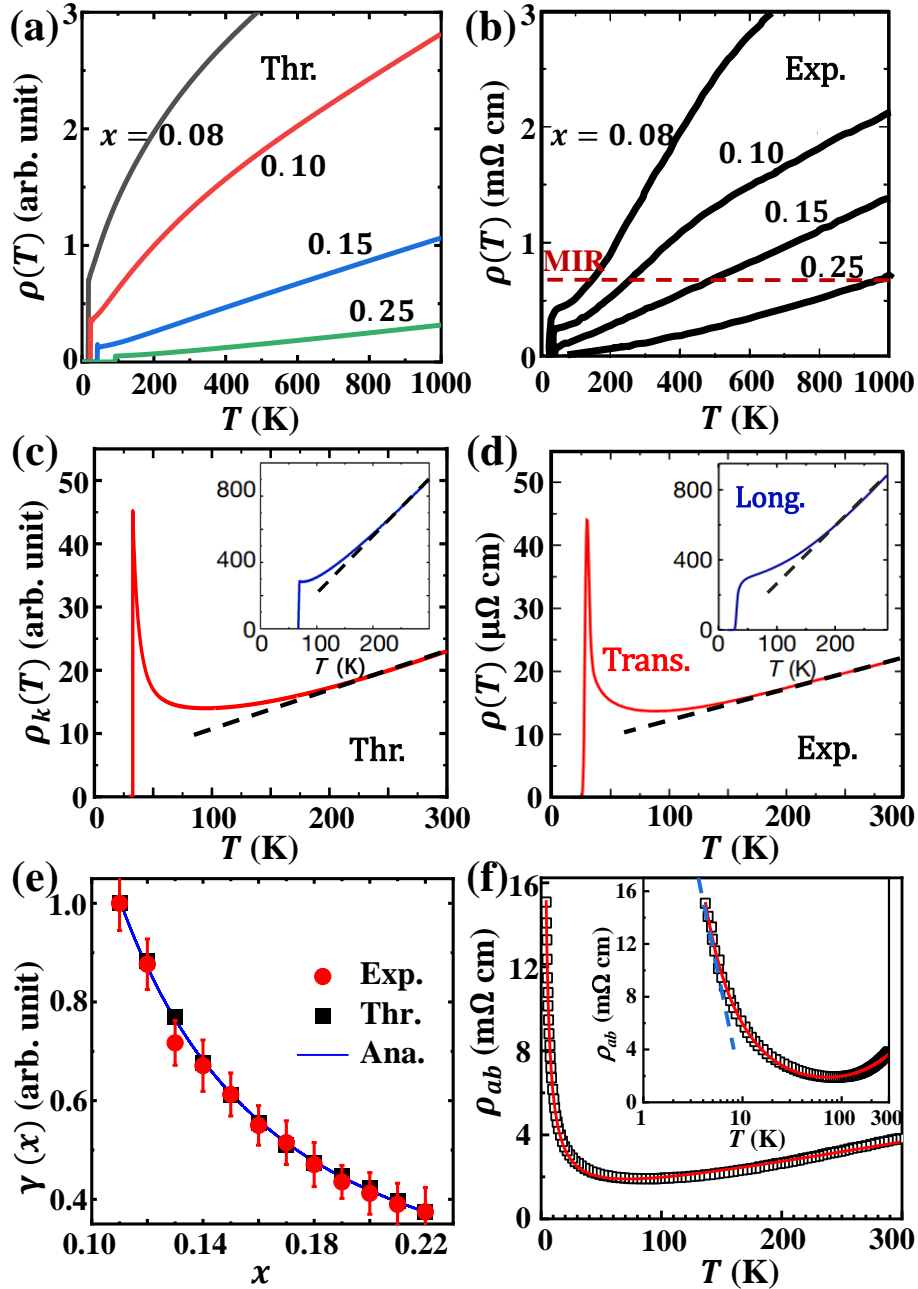


Figure 3: (a) Drude weight representing transport in the EBL and (b) experimental transport observations with generally good agreement. In particular, both share linear resistivity over a broad range of temperatures, ignorance of the MIR bound, and general doping dependence trends. (c) At lower temperatures, the linear resistivity gives way to weak insulating behavior in excellent agreement with experiments (47). (e) Careful analysis of the doping dependent resistivity slope agrees with observations (58) up to a doping-independent shift accounting for e.g. phonon scattering. (f) The Drude weight in our EBL (red line) provides an excellent phenomenological fit for the experimental in-plane resistivity of LSCO (59) over a broad temperature range including the well-known $\ln(1/T)$ behavior at low-temperature (dashed blue line).

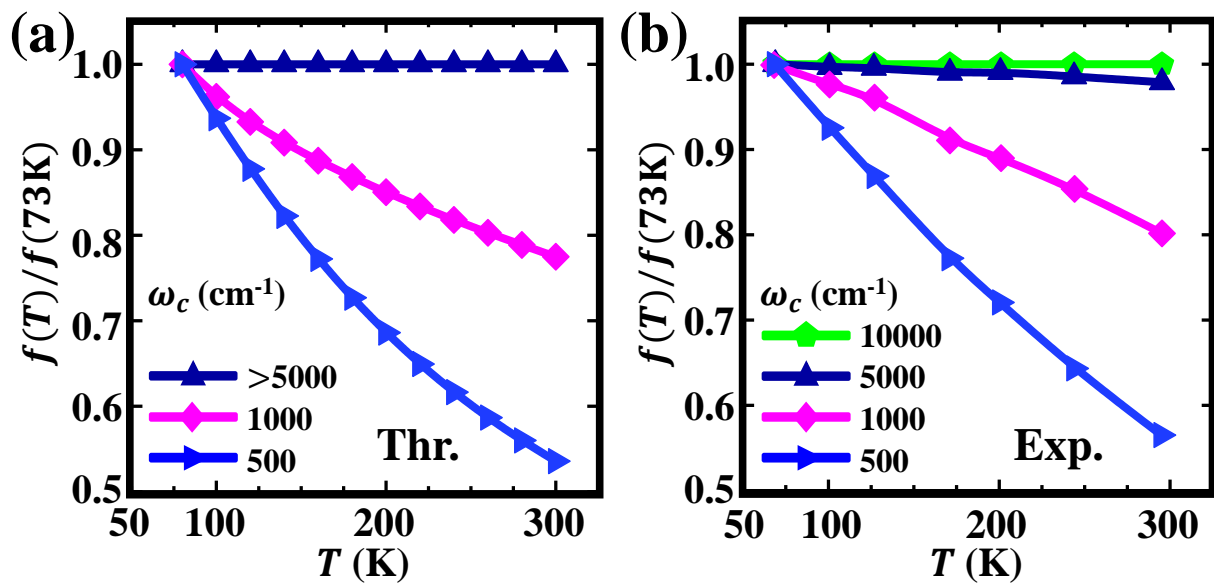


Figure 4: Temperature-dependent fraction $f(T)$ of integrated spectral weights in (a) our EBL model and (b) observations of Bi-2212 (28) closely match. The spectral weight quickly transfers to higher frequency with increasing temperature as indicated by the steep negative slopes for lower cutoff ω_c .

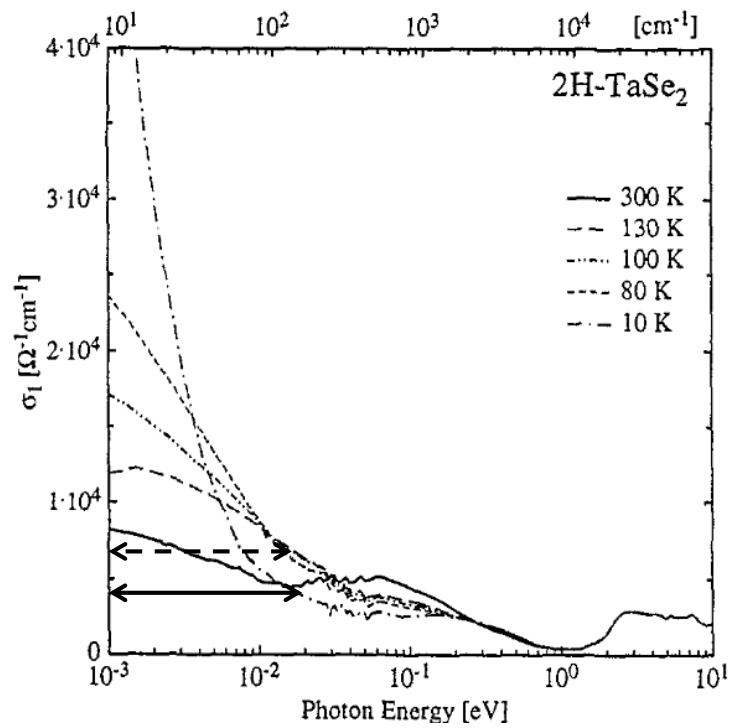


Figure S1: Optical conductivity for transition-metal dichalcogenide 2H-TaSe₂ (*I*) indicating that the full-width at half-max (FWHM) of the low frequency peak does not change appreciably from 130K up to room temperature.

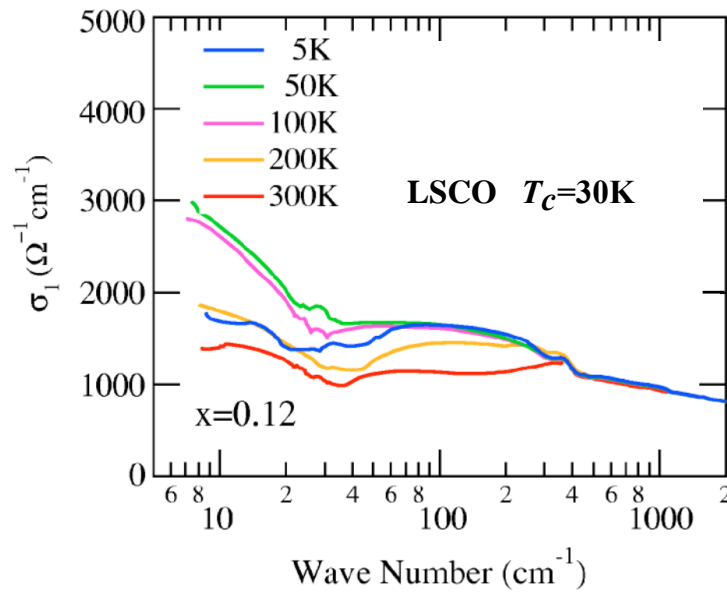


Figure S2: Optical conductivity for cuprate LSCO (2) indicating that the FWHM of the low-frequency peak does not change appreciably from e.g. 200K up to room temperature.

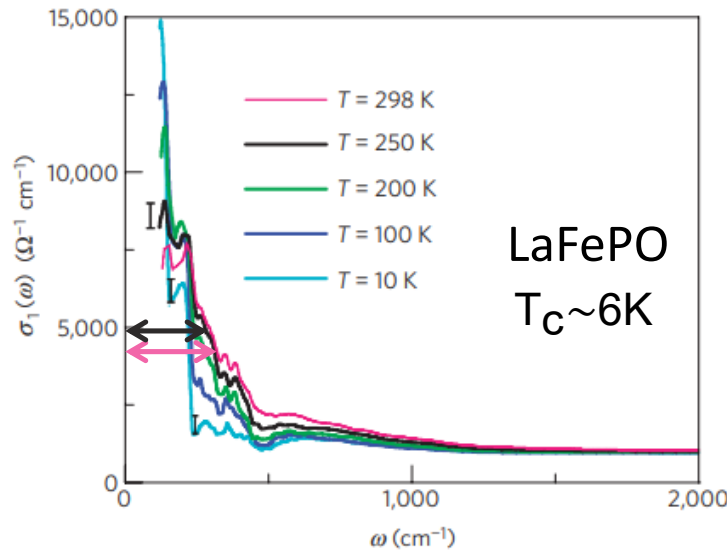


Figure S3: Optical conductivity for iron-based superconductor LaFePO (3) indicating that the FWHM of the low frequency peak is similar for temperatures from 250K up to room temperature.